Ab initio investigation of phonon-mediated superconductivity in the ternary borides Mo_5XB_2 (X = P, Si, Ge): Comparison with W_5SiB_2

S. Bağcı,[1] H. M. Tütüncü,[1] H. Y. Uzunok,[1] and G. P. Srivastava[2]
[1]*Sakarya Üniversitesi, Fen Fakültesi, Fizik Bölümü, 54050 Sakarya, Turkey*
[2]*Department of Physics and Astronomy, University of Exeter, Stocker Road, Exeter EX4 4QL, United Kingdom*

(Received 13 February 2024; revised 4 April 2024; accepted 11 April 2024; published 30 April 2024)

In this work, we have investigated the elastic and mechanical properties, electronic band structure, lattice dynamics, and electron-phonon interaction in four ternary transition metal borides Mo_5PB_2, Mo_5SiB_2, W_5SiB_2, and Mo_5GeB_2 by executing systematic *ab initio* calculations based on density functional theory within the generalized gradient approximation. The calculated elastic constants and elastic moduli for Mo_5SiB_2 agree well with available experimental data. The calculated elastic constants and phonon dispersion relations show that all the considered borides are mechanically and dynamically stable. The electronic density of states near the Fermi level of these compounds is dominated by the transition metal d orbitals, which leads to low-frequency phonon modes arising from the vibrations of transition metal atoms being more strongly involved in the process of scattering of electrons rather than high-frequency phonon modes arising from the vibrations of lighter other two atoms. Our electron-phonon interaction calculations reveal that the electron-phonon coupling strength of Mo_5PB_2 is the strongest with a value of 0.959 among all the studied compounds, which in turn yields a superconducting transition temperature (T_c) value of 9.527 K, being higher than the T_c values of Mo_5SiB_2 (5.845 K), W_5SiB_2 (5.931 K), and Mo_5GeB_2 (6.193 K). All these T_c values harmonize with their respective experimental values of 9.2, 5.8, 5.8, and 5.8 K, indicating the reliability of our *ab initio* calculations.

DOI: 10.1103/PhysRevB.109.144524

I. INTRODUCTION

Transition metal borides have always been at the center of scientific research, which is due to their heat-resistant nature, high melting points, high hardness, good electrical and thermal conductivities, and low coefficient of friction [1]. Because of these properties, such materials are widely used in cutting tools, heat resistant crucibles, wear-resistant coatings, solar panels, permanent magnets, and materials resistant to oxidation at high temperatures [2–16]. Ternary borides with 512 stoichiometries of M_5XB_2 (X = P, Si) are the most interesting subgroup among the transition metal borides. These ternary compounds contain 3d transition metals from V to Co, 4d transition metals Nb and Mo, and 5d transition metal W. For example, Mn_5SiB_2 and Mn_5PB_2 exhibit ferromagnetic behavior with their Curie temperatures close to room temperature [7,8]. In addition, Fe_5SiB_2 and Fe_5PB_2 are reported to be uniaxial ferromagnets with their high Curie temperatures and have been investigated as potential permanent magnets [13,14]. Above all, the discovery of superconductivity in MgB_2 at 39 K [17] encouraged researchers to find new superconductors containing boron. Mo_5SiB_2 was found to be superconducting at 5.8 K in 2011 [18]. Before the discovery of superconductivity, the structural, elastic, and mechanical properties of Mo_5SiB_2 material were experimentally investigated by different groups [19–22]. Experimental studies [19,20] on mechanical properties have revealed that this superconductor is durable and ductile. Mo_5SiB_2 is thus a promising material for technological applications. However, because their brittle nature, high-temperature superconductors are not widely used in technology [23,24]. Above all, the superior mechanical properties and machinability of Mo_5SiB_2 enable it to be used in high temperature applications [10,16,25]. Later it was determined that W_5SiB_2 also has a Cr_5B_3 crystal structure, and it also shows superconductivity around 6 K [26]. The observation of superconductivity in W_5SiB_2 is technologically interesting because it is resistant to thermal shock and is a good thermal conductor. Observing superconductivity in different samples of compounds with Cr_5B_3 type and the 5:1:2 elemental ratio has shed light on the production and study of this new type of superconductors in recent years. Experimental studies for one of these materials, Mo_5PB_2, have shown that it is superconducting at 9.2 K [27]. This temperature is the highest superconductivity transition temperature for compounds belonging to this group. Another experimental study [28] conducted in 2020 confirmed that this compound is a multigap superconductor. These experimental studies show that when the P atom replaces the Si atom with four valence electrons in Mo_5SiB_2 with five valence electrons, the superconductivity transition temperature increases by about 4 K. In order to determine the physics behind this temperature increase, the electronic, phonon and electron-phonon interaction of these materials must be studied theoretically and the physics of the superconductivity mechanism must be determined. In 2021, Xu and coworkers prepared polycrystalline Mo_5GeB_2 by replacing the Si atom in Mo_5SiB_2 with the heavier Ge atom. This group has measured this material's electrical conductivity, magnetization, and heat capacity and shared its superconductivity parameters with the scientific world. According to this experimental study [29],

Mo_5GeB_2 is a type II superconductor with a transition temperature of 5.4 K. In another experimental study [30] conducted in 2021, the transition temperature of this superconductor was determined as 5.8 K, equal to the experimentally measured transition temperature of Mo_5SiB_2. This result signals no significant change in the superconductivity transition temperature with the replacement of Si and Ge atoms with the same valence electrons.

Experimental discovery of superconductivity in transition metal borides with Cr_5B_3 tetragonal crystal structure triggered theoretical studies on them. As far as we know, the first theoretical work on these superconductors is the examination of the electronic structure of W_5SiB_2 by using the density functional theory [26]. This theoretical study reveals that the electronic states near the Fermi energy are mainly dominated by the d electrons of the transition metal atom, signaling that they play a crucial role in the formation of superconducting state for W_5SiB_2. The second theoretical study we encountered has been carried out on the thermodynamic properties of Mo_5SiB_2 using the generalized gradient approximation (GGA) of the density functional theory [31]. This theoretical approach was used in the work of McGuire and Parker in 2016 to examine the electronic band structures of Mo_5PB_2 and Mo_5SiB_2 compounds [27]. The experimental determination of the elastic and mechanical properties of Mo_5SiB_2 triggered theoretical studies on it. Aryal and coworkers [32] have investigated the mechanical, elastic and vibrational properties of this compound by using the generalized gradient approach, and the calculated mechanical results are found to be in agreement with the experimental data [19,20]. In 2020, the elastic, mechanical and electronic properties of Mo_5SiB_2 have been also studied by Pan and Pu [33]. This theoretical research has once again confirmed that this superconductor is durable and ductile [33]. In addition to the electronic properties of Mo_5SiB_2, the electronic properties of Mo_5PB_2, which has the highest transition temperature in this group, have been analyzed with the GGA approach and it is found that the electronic density of states at the Fermi level is mainly dominated by Mo 4*d* electrons. Another superconducting compound whose electronic properties have been studied theoretically is Mo_5GeB_2. This GGA work [29] emphasized that six electronic bands traversed the Fermi level and as a result, Mo_5GeB_2 has metallic character. Naher and co-workers [34] have investigated a large number of hitherto unexplored properties of Mo_5PB_2 in details, such as elastic, electronic, thermophysical, bonding and optoelectronic properties. According to this theoretical study [34], this compound is machinable, ductile and possesses significant hardness. In 2022, the variation of the mechanical properties of Mo_5SiB_2 with pressure have been examined by using the GGA method and it is noted that the values of both the bulk modulus and the shear modulus increase with pressure [35].

Although the above literature research shows that Cr_5Si_3-type superconductors, which have the superior properties of both metals and ceramics, have been kept up-to-date since the day they were discovered, their electron-phonon interaction properties have not been systematically examined. However, it is a notable deficiency that the electron phonon properties of these materials have not been studied because when studying systems in the metallic state, many physical properties, such as electrical and thermal resistivities, thermal expansion, and superconductivity, seem to be governed by phonons and their interactions with electrons. Thus, in this study, it is planned to systematically examine the physical and electron-phonon interaction properties of Mo_5SiB_2, Mo_5GeB_2, Mo_5PB_2, and W_5SiB_2 (All is abbreviated as T_5XB_2 in this paper) superconductors, thus determining which phonon modes play important role in the transition from the normal state to the superconducting state. First, we have realized first-principles calculations on the structural and electronic properties of these superconductors by using a generalized gradient approximation of density functional theory [36,37]. Their structural and electronic properties are determined and compared with each other in detail. Secondly, we have performed a detailed investigation on the elastic properties of these superconductors by using the influential stress-strain method [38]. Thus the calculated elastic constants of Mo_5SiB_2 are interpreted by comparing them with the experimental data. Thirdly, the isotropic bulk modulus, the isotropic shear modulus, Poisson's ratio, and Young's modulus for these superconductors are determined by using the values of calculated elastic constants with the help of the Voigt–Reuss–Hill (VRH) scheme [39–42]. Afterwards, the strength and ductility of the examined superconductor using these elastic moduli are determined and discussed them in detail. Fourthly, due to the significant role of phonons in the formation of Cooper pairs, we have conducted phonon calculations on these superconductors by utilizing the density functional perturbation theory within the linear response approach [36,37]. Afterwards, the calculated phonon dispersion curves as well as the phonon density of states for these superconductors are compared between each other in detail. In the final step of this theoretical calculation, electron-phonon interaction calculations for all the examined compounds have been performed by combining the linear response approach [36,37] and the Migdal-Eliashberg approach [43,44]. Afterwards, the calculated Eliashberg functions of examined superconductors are compared in detail with their electronic and phonon density of states and thus it will be determined from which phonon modes and which electronic orbitals the superconductivity mechanism originates. Furthermore, the Eliashberg spectral functions of these superconductors have been used to calculate their electron-phonon coupling parameters and their logarithmic average of phonon frequencies. Using these physical quantities, their superconducting transition temperatures are determined and compared with their corresponding experimental values.

The rest of this study are organized as follows. In the next section we shall briefly report the method and parameters we employed in our *ab initio* calculations. In continuation we elucidate our electronic results, concentrating on the electronic band structure, electronic density of states, and Fermi surfaces. These results are followed by a detailed analysis of elastic and mechanical properties, focusing on the mechanical stability, hardness, ductility and machinability of the studied compounds for their possible technological application. Following that, we report our results for phonon and electron-phonon interaction properties, focusing on the phonon spectrum, phonon density of states and the Eliashberg spectral function. Finally, we summarize our work.

II. THEORY

The *ab initio* structural optimizations, elastic constants, electronic band structures and density of states calculations are based on density functional theory (DFT) [45,46] with the generalized gradient approximation (GGA) of Perdew-Burke-Ernzerhof [47]. The calculations have been performed by using the plane-wave pseudopotential method, as implemented in the QUANTUM ESPRESSO simulation package [36,37]. The electron-ion interaction is described by the ultrasoft pseudopotentials of Vanderbilt-type [48]. The plane-wave cutoff energy is set to 60 Ry for all the studied borides while the electronic charge density is expanded up to 600 Ry. The Kohn-Sham equations [46] have been solved using an iterative conjugate gradient scheme, employing a set of Monkhorst-Pack special $\boldsymbol{k}$ points [49]. For the Brilllouin zone (BZ) integration, the Gaussian method is utilized with a Γ-centered $\boldsymbol{k}$-point mesh of (8×8×8) for the *ab initio* structural optimizations. The electronic properties are investigated by using a denser $\boldsymbol{k}$-point mesh of (24×24×24).

We have calculated the phonon dispersion relations and phonon density of states using the *ab initio* density functional perturbation theory (DFPT) as implemented in the QUANTUM ESPRESSO simulation package [36,37]. Since phonon structure calculations are much more time consuming than electronic structure calculations, thirteen dynamical matrices on the (4×4×4) Monkhorst-Pack grid are calculated. Then, through double Fourier interpolation, real space inter-atomic force constants are obtained from these dynamical matrices and utilized to compute the phonon dispersion relations as well as phonon density of states. The electron-phonon interaction properties have been analyzed based on the density functional perturbation [36,37] and Eliashberg theories [43,44]. For superconductors with the dominant electron-phonon interaction, the superconducting properties can be examined through calculating the Eliashberg spectral function $\alpha^2F(\omega)$, being given as

$$\alpha^2F(\omega) = \frac{1}{2\pi N(E_F)} \sum_{\boldsymbol{q}j} \frac{\gamma_{\boldsymbol{q}j}}{\hbar\omega_{\boldsymbol{q}j}} \delta(\omega - \omega_{\boldsymbol{q}j}), \tag{1}$$

where $N(E_F)$, $\gamma_{\boldsymbol{q}j}$ and $\omega_{\boldsymbol{q}j}$ refer to the electronic density of states at the Fermi level, the phonon linewidth due to electron-phonon scattering, and the phonon frequency of branch index j at wave vector $\boldsymbol{q}$, respectively. The strength of the electron-phonon coupling in a superconductor is measured by the electron-phonon coupling constant (λ), which can be derived from the Eliashberg spectral function ($\alpha^2F(\omega)$) via the Allen-Dynes formula [50–52]

$$\lambda = 2\int_0^\infty \frac{\alpha^2F(\omega)}{\omega} d\omega. \tag{2}$$

Now, the logarithmically averaged phonon frequency (ω_{ln}) can be calculated using λ and the $\alpha^2F(\omega)$ function with the following formula:

$$\omega_{ln} = \exp\left(2\lambda^{-1}\int_0^\infty \frac{d\omega}{\omega}\alpha^2F(\omega)\ln\omega\right). \tag{3}$$

Finally, using the calculated λ and ω_{ln}, we can estimate the superconducting transition temperature T_c via McMillan-Allen-Dynes formula [50–52]

$$T_c = \frac{\omega_{\ln}}{1.2}\exp\left(-\frac{1.04(1+\lambda)}{\lambda - \mu^*(1+0.62\lambda)}\right). \tag{4}$$

Here, μ^* is the averaged screened electron-electron interaction, and its value remains between 0.10 and 0.20 [50–53]. In our calculations, the value of μ^* is taken to be 0.16.

III. RESULTS AND DISCUSSION

A. Structural and electronic properties

The crystal structure of the studied ternary borides is displayed in Fig. 1. All the investigated compounds with the formula of T_5XB_2 exist in the body-centered tetragonal Cr_5B_3-type crystal structure, with space group No. 140 (I4/mcm) and two formula unit per primitive cell. There are four inequivalent atomic positions: two T1 atoms (Mo or W) at (4c) site (0, 0, 0), eight T2 atoms (Mo or W) at (16l) site (x_{T2}, x_{T2}+1/2, z_{T2}), two X atoms at (4a) site (0, 0, 1/4), and four B atoms at (8h) site (x_B, x_B+1/2, 0), where (x_{T2} and z_{T2}) and x_B are the internal coordinates of T2 and B atoms, respectively. Clearly, the crystal structure is governed by two lattice parameters (a and c) and three inner coordinates (x_{T2}, z_{T2}, and x_B). At the first stage of our first principles calculations, the full structural optimization of all the studied compounds has been performed both over the lattice parameters and the atomic positions including the internal coordinates. Therefore the equilibrium values of volume, lattice parameters (a and c) and inner coordinates (x_{T2}, z_{T2}, and x_B) for all the studied compounds are determined. Having determined the equilibrium volume, the total energies are calculated as a function of volume and fitted to Murnaghan equation of state [54] to obtain the bulk modulus (B), and its pressure derivative (B'). The obtained values of volume (V), lattice parameters (a and c), inner coordinates (x_{T2}, z_{T2}, and x_B), bulk modulus (B), and its pressure derivative (B′) of each compounds are presented and compared with previous theoretical results [33,34] and available experimental data [18,21,22,26,27,29] in Table I. In general, the calculated values of volume, lattice parameters and inner coordinates for all the investigated compounds agree satisfactorily with their experimental values [18,21,22,26,27,29]. In general, the calculated lattice parameters of all the studied compounds are slightly larger than the experimental lattice constants, which is a typical error of the application of the GGA scheme. In general, Table I indicates that all the studied borides are hard compounds with their bulk moduli being larger than that of a hard compound sapphire ($B^{Al_2O_3} = 246$ GPa), implying that they are incompressible compounds [55]. In particular, the bulk modulus of W_5SiB_2 is only about 20% lower than that of a superhard compound cubic boron nitride ($B^{c-BN} = 369$ GPa) [56].

The electronic structures of the examined T_5XB_2 materials are shown in Fig. 2. A total of six bands cut the Fermi level in all the materials examined. This is in agreement with previous studies [27,28]. Of these, the band with the lowest energy is shown in color magenta, while the band with the highest energy is shown in brown. With reference to the Fermi energy, these bands are spread between −1.0 and

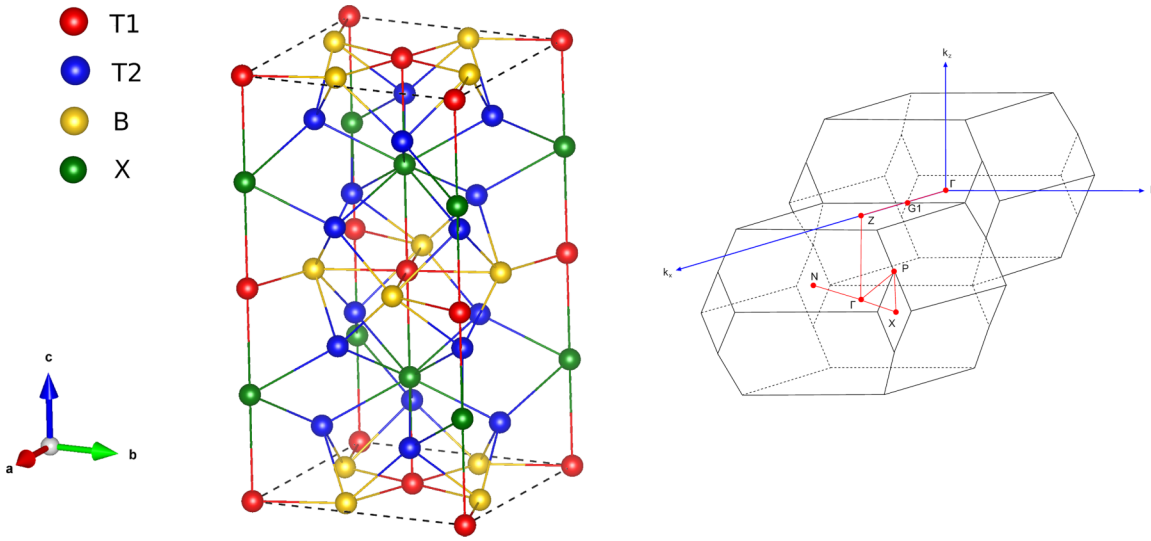

FIG. 1. The body centered crystal structure of all the studied borides and the Brillouin zone of body-centered tetragonal lattice. T1 and T2 = Mo or W and X = Si, Ge, or P.

0.9 eV for Mo_5GeB_2, −1.1 to 1.1 eV for Mo_5PB_2, −1.1 to 1.0 for Mo_5SiB_2, and −1.3 to 1.1 for W_5SiB_2. The material with the widest bandwidth is W_5SiB_2 with $\Delta E = 2.4$ eV. While Mo_5GeB_2 and W_5SiB_2 do not have bands that cut off the Fermi level in the N-P direction, some bands do so for Mo_5PB_2 near the P point in this direction and for Mo_5SiB_2 near the N point. Since the electron-phonon interaction is sensitively influenced by the Fermi surface topology [57,58], it would be a good idea to investigate these surfaces. The Fermi surfaces resulting from these bands are created via the XCRYSDEN software [59] and are shown in Fig. 3. The Fermi surfaces formed by the magenta band nest in the direction N-P with a similar complex structure for Mo_5GeB_2, Mo_5PB_2, and W_5SiB_2, while the Mo_5SiB_2 compound shows a nesting in the direction of Γ-X. The nesting blue and cyan bands in the Γ-Z direction is expected to contribute to electron scattering. Both bands form closed curves around the Γ point. Green bands form closed curves around the point Z while slotting in the Γ-Z direction and the Z-G1 direction which could enhances the electron-phonon interaction.

The total and partial state densities (DOS) of the compounds studied are shown in Fig. 4. The data obtained from these figures also agree with the previous values [27,28]. The valence for the Mo_5GeB_2 compound can be examined in three bands of the DOS region. However, since BCS theory states that Cooper pairs are formed by electrons whose energies are close to the Fermi level, we will only focus our attention around this level. As can be seen from Fig. 4, the near-Fermi DOS of Mo_5GeB_2 shows a dominance of Mo 4d shell. The Fermi level DOS value (N(E_F)) for this compound is found to be 10.74 states/eV, 90% of which comes from the 4d shell of the Mo atom. As a result, we can say that the superconductivity of this compound is governed by Mo 4d electrons because of their dominance around the Fermi level.

Similar to Mo_5GeB_2, the valence band spectrum of Mo_5PB_2 and Mo_5SiB_2 can be examined in three parts (see Fig. 4). In agreement with Mo_5GeB_2, the most significant contribution to the Fermi level of the compounds Mo_5PB_2 and Mo_5SiB_2 comes from the 4d shell of the Mo atom. The ratio of this contribution to N(E_F), which has a value of 10.70

TABLE I. The calculated values of volume (V), lattice parameters (a and c) and inner coordinates (x_{T2}, z_{T2}, and x_B) for all the studied compounds and their comparison with previous experimental and theoretical results.

Superconductor	V (Å^3)	a (Å)	c (Å)	x_{T2}	z_{T2}	x_B	B (GPa)	B'
Mo_5PB_2	199.505	5.988	11.128	0.16620	0.14009	0.61858	275.10	4.29
Experimental [27]	197.578	5.973	11.076	0.16593	0.14102	0.61840		
GGA [34]	197.272	5.970	11.070	0.16590	0.1410	0.6180		
Mo_5SiB_2	202.899	6.042	11.116	0.16426	0.13912	0.62117	268.90	4.51
Experimental [21]	198.354	5.998	11.027	0.16530	0.1388	0.62500		
Experimental [22]	201.003	6.027	11.067	0.16411	0.13981	0.62158		
Experimental [18]	198.462	6.001	11.022					
GGA [33]	199.437	6.013	11.032	0.1653	0.1388	0.6653		
Mo_5GeB_2	207.601	6.099	11.162	0.15957	0.13690	0.62678	254.90	5.01
Experimental [29]	205.214	6.075	11.121	0.16188	0.13834	0.63577		
W_5SiB_2	204.909	6.093	11.039	0.16031	0.14056	0.62837	302.00	4.83
Experimental [26]	200.760	6.034	11.028					

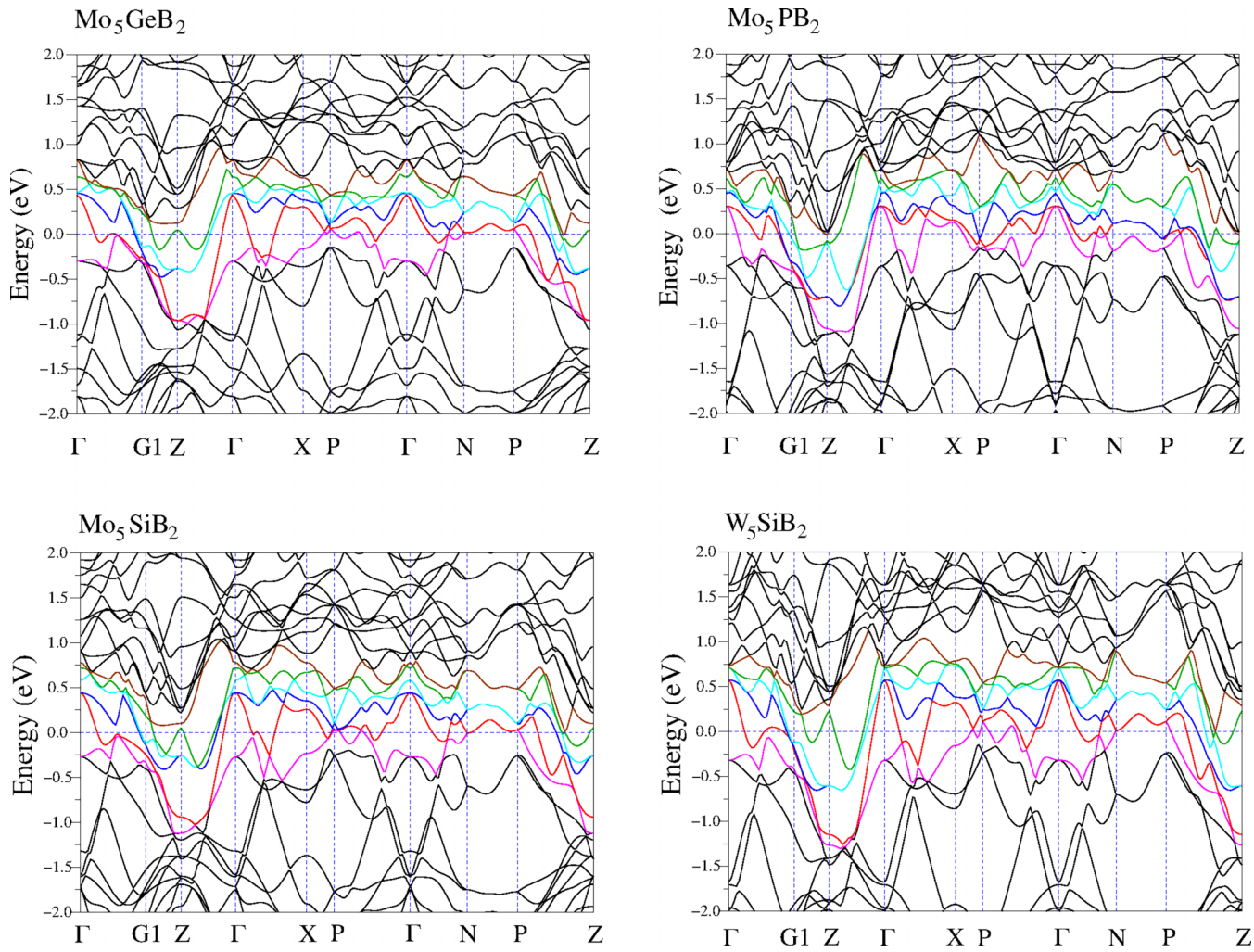

FIG. 2. The calculated electronic structure of all the studied compounds.

states/eV for Mo_5PB_2 and 10.40 states/eV for Mo_5SiB_2, is 91% for the Mo_5PB_2 compound and 87% for the Mo_5SiB_2 compound. As can be seen, in Mo_5XB_2 compounds, when the Si atom comes in place of X, the valence band spectrum gradually narrows and disappears between the gaps. When the P atom is substituted for X, the energy range expands, and the separation between the bands becomes apparent.

A different DOS graph is obtained for the W_5SiB_2 compound than in the compounds previously studied. The gaps that are narrow in the Mo_5SiB_2 compound disappear with the substitution of the W atom in the Mo place, resulting in a gapless valence band spectrum. This band, which starts at −12.8 eV, is dominated by the W 6p orbitals up to −9.2 eV, while after this value, the contribution from the W 5d shell gives the largest contribution to the whole DOS. The W 5d shell also closes the gap between the separated bands, which could be seen in the previously mentioned Mo-based compounds. The N(E_F) value for W_5SiB_2 is calculated as 8.63 states/eV, and 86% of the $N(E_F)$ value comes from the W 5d shell. According to BCS superconductivity theory, the Cooper pairs are formed by the free electrons with the energies near the E_F. Hence, it could be said that the studied compounds show superconductivity due to the d shells of Mo and W atoms.

B. Elastic and mechanical properties

The elastic constants presented here are obtained from the application of the linear finite strain-stress method as implemented in the THERMO$_{pw}$ code [38]: a set of small strains is applied to the crystal lattice, and then the lattice, including the atoms, relaxed to determine the corresponding stress. Later on, single-crystal elastic constants are deducted from the determined strain-stress relations. A tetragonal system has six independent second-order elastic constants, which are C_{11}, C_{12}, C_{13}, C_{33}, C_{44}, and C_{66}. Their calculated values for all the compounds under study are presented in Table II, together with available experimental and GGA results for Mo_5SiB_2 [20,33] and previous the GGA results for Mo_5PB_2 [34].

First of all, the calculated values of second-order elastic constants for Mo_5SiB_2 are in satisfactory accordance with their experimental values [20] with reduction no more than 7%. Second, our calculated results for Mo_5SiB_2 and Mo_5PB_2 are comparable with previous GGA results [33,34]. Third, our results presented for the second-order elastic constants of two remaining superconductors in Table II are totally new and must be treated as predictions since there are no experimental or theoretical counterparts available at this moment to our knowledge.

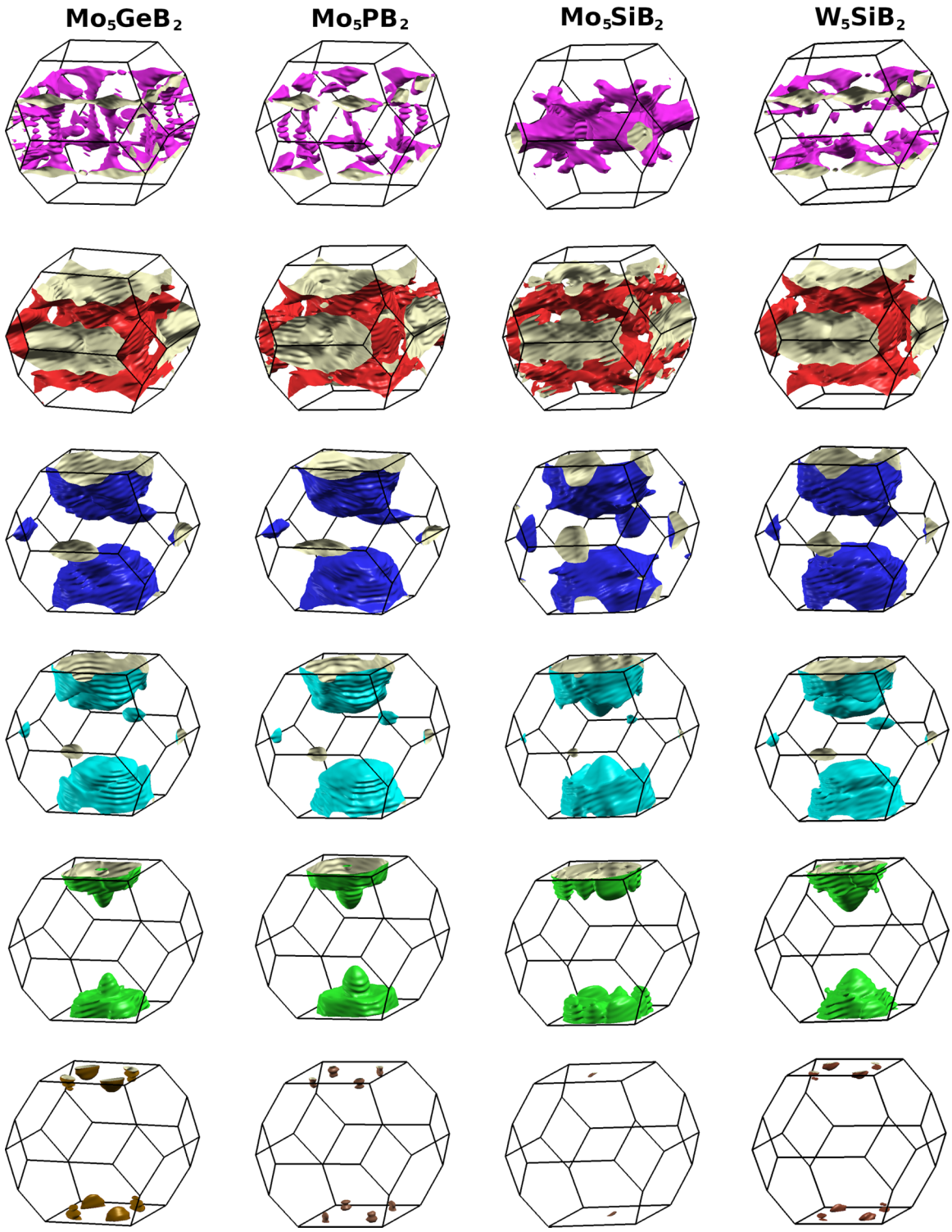

FIG. 3. The calculated Fermi surfaces of all the investigated compounds.

C_{11} and C_{33} represent the resistance to linear compression under stress along the x-axis and z-axis directions, respectively while C_{44} and C_{66} can be related to shear deformation. For all the studied compounds, the elastic constant C_{11} has a larger value than the elastic constant C_{33}, signaling that the deformation resistance along [100] direction is higher than [001] direction. Furthermore, for all the investigated compounds, the elastic constants C_{44} and C_{66} are significantly lower than the elastic constants C_{11} and C_{33}, indicating that the compression resistance of studied compounds is higher than their resistance to shear deformations.

The confirmation of mechanical stability is essential for studying the mechanical properties of a compound. Mechanical stability of a tetragonal compound requires that its independent elastic constants must satisfy the following

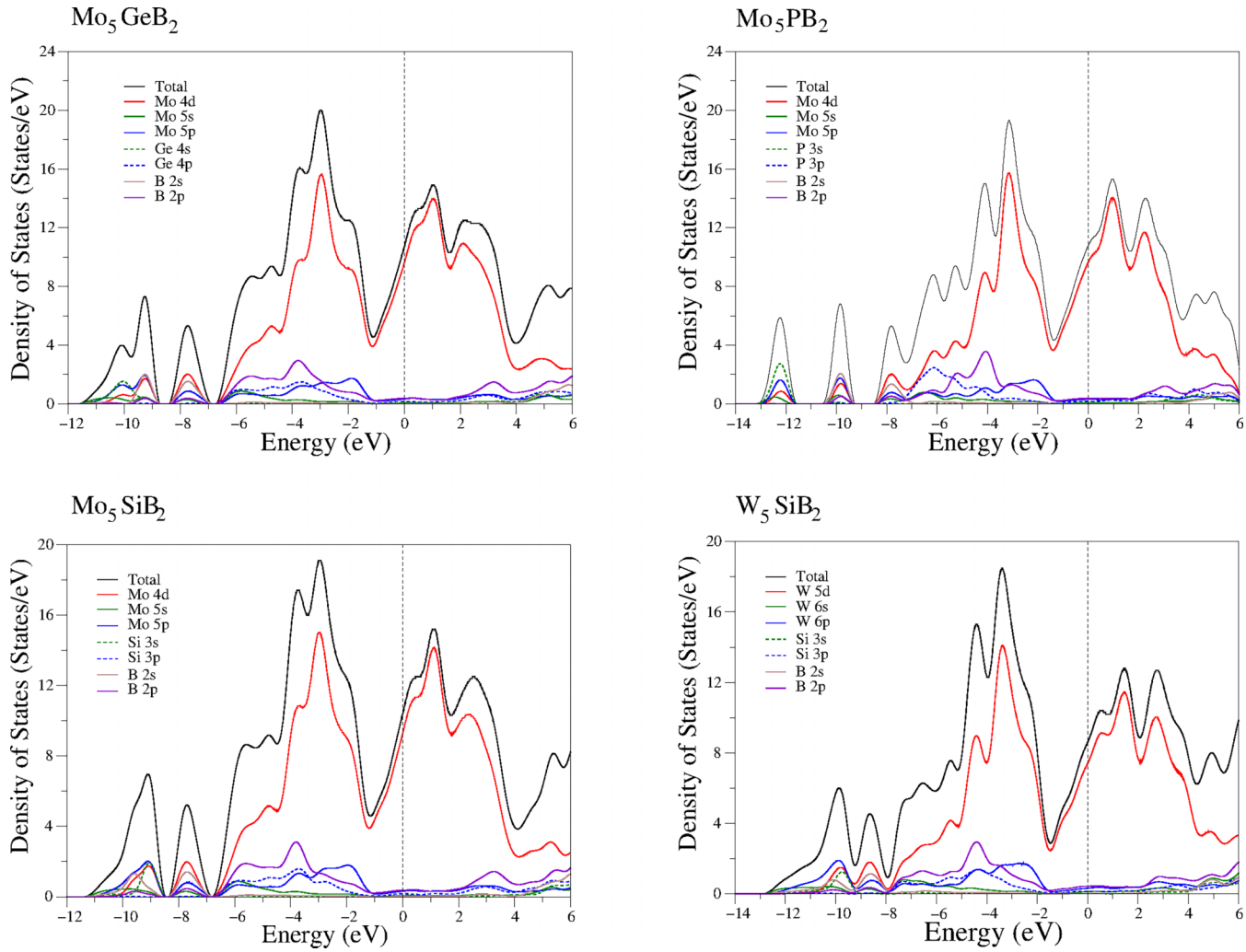

FIG. 4. The calculated density of states of all the studied borides.

Born's stability criteria:

$$C_{11} > 0,\ C_{33} > 0,\ C_{44} > 0\, C_{66} > 0,$$
$$(C_{11} - C_{12}) > 0,\ (C_{11} + C_{33} - 2C_{13}) > 0,$$
$$(2C_{11} + 2C_{12} + C_{33} + 4C_{13}) > 0.$$

It can be seen that all the studied compounds are mechanically stable in their Cr_5B_3-type crystal structure because their calculated elastic constants meet the above mechanical stability criteria.

The dynamical stability of a crystalline compound can be judged by analysing its shear constant $[C' = (C_{11} - C_{12})/2]$. When its value becomes positive, the compound is dynamically stable, otherwise it is dynamically unstable. As can be extracted from Table II, the shear constant of all the studied compounds takes only positive value, indicating that they are all dynamically stable. The Cauchy pressure is assumed to determine the bonding nature in a compound depending on its value (either positive or negative). Its negative value points toward covalent bonding with brittle nature, while its positive

TABLE II. The calculated values of second order elastic constants (in GPa) for all the studied compounds, together with available experimental results for Mo_5SiB_2 and previous GGA results for Mo_5SiB_2 and Mo_5PB_2.

Superconductor	C_{11}	C_{12}	C_{13}	C_{33}	C_{44}	C_{66}
Mo_5PB_2	460.43	172.50	215.65	361.42	135.03	134.48
GGA [34]	478.70	168.93	206.31	379.68	142.86	138.38
Mo_5SiB_2	467.00	162.17	195.11	388.92	162.53	137.52
Experimental [20]	480	166	197	415	174	143
GGA [33]	483	165	188	398	172	152
W_5SiB_2	487.83	183.33	233.25	454.36	183.21	125.68
Mo_5GeB_2	427.06	157.79	198.58	344.38	150.89	115.08

TABLE III. The calculated values of isotropic bulk modulus B_{VRH}, shear modulus G_{VRH}, Young's modulus E (all in GPa), B_H/G_H ratio, Poisons's ratio σ and hardness H (in GPa) for all the studied compounds calculated from the corresponding second order elastic constants C_{ij}.

Superconductor	B_V	B_R	B_H	G_V	G_R	G_H	E	B_H/G_H	σ	H
Mo_5PB_2	276.65	275.25	275.95	126.14	120.71	123.43	322.22	2.236	0.305	18.936
GGA [34]	277.80	276.35	277.07	135.19	131.40	133.30	344.63 E	2.083	0.290	20.682
Mo_5SiB_2	269.75	269.02	269.39	143.89	139.90	141.89	362.09	1.898	0.276	22.201
Experimental [20]			277			151	383	1.834		23.813
GGA [33]			271			152	384	1.78	0.385	23.998
W_5SiB_2	303.29	303.20	303.25	150.43	144.01	147.22	380.13	2.059	0.291	23.144
Mo_5GeB_2	256.49	255.67	256.08	126.28	119.25	122.77	327.52	2.086	0.293	18.820

value corresponds to metallic bonding with ductile nature [60]. Different from a cubic system, there are two Cauchy pressures $C_{12} - C_{66}$ and $C_{13} - C_{44}$ for a tetragonal system. As can be derived from Table II, both Cauchy pressures of all the studied compounds have positive values, indicating the dominating nature of metallic bonding and the ductile nature for them. The ductile nature of these ternary compounds is excellent information for their possible technological applications because the brittle nature of high temperature superconductors prevents them from being widely used in technology [23,24].

The calculated values of second-order elastic constants have been used to get the isotropic bulk modulus (B_{VRH}) and the isotropic shear modulus (G_{VRH}) in the framework of the Voight-Reuss-Hill (VRH) approximation for polycrystalline aggregates [39–42]. Then, the Young's modulus (E) and Poisson's ratio (σ) are also determined by using the following equations:

$$E = \frac{9B_H G_H}{3B_H + G_H}, \tag{5}$$

$$\sigma = \frac{3B_H - 2G_H}{6B_H + 2G_H}. \tag{6}$$

Our GGA results for the values of bulk modulus B_{VRH}, shear modulus G_{VRH}, Young's modulus E(all in GPa), B_H/G_H ratio and Poissons's ratio σ for all the studied compounds are tabulated in Table III, together with available experimental results for Mo_5SiB_2 and previous GGA results [34] for Mo_5PB_2. The calculated values of B_H, G_H, and E for Mo_5SiB_2 are slightly smaller than their corresponding experimental values with the maximum variation of 6% for G_H. Furthermore, our GGA results compare very well with previous GGA results for the elastic moduli of Mo_5PB_2. Although previous results are not available for the other two superconductors, a comparison of Tables I and III reveals that the calculated bulk moduli of all the examined compounds determined from the total energy minimization and from the elastic constants have almost the same values which also gives a further support for the validity of our theoretical calculations. The calculated elastic moduli signal that all the borides are hard compounds. In particular, the calculated bulk modulus (B) and the shear moduli (G) of all the studied borides are comparable to those of several hard compounds, such as ZrC (223 GPa, 116 GPa), VN (268 GPa, 159 GPa), NbN (315 GPa, 156 GPa), B_4C (247 GPa, 171 GPa), and Al_2O_3 (246 GPa, 162 GPa) [55]. The two main mechanical parameters of polycrystalline compounds are bulk and shear moduli. The bulk modulus (B) is the main tool to evaluate the mechanical behavior of solids as it reflects the ability of solids to resist volume, while the shear modulus (G) reflects the resistance of compounds against shape change caused by a shearing force. Therefore the results presented in Table III suggest that the considered ternary compounds are more resistive to volume compression than shear, due to the fact that $B_H > G_H$. The Young's modulus (E) of a compound is identified as the ratio of linear stress to linear strain and can then procure useful information about its stiffness. The calculated Young's moduli (E) of the examined compounds are above 320 GPa, and consequently, they can be classified as relatively stiff compounds. In particular, the calculated bulk modulus, shear modulus and Young's modulus of W_5SiB_2 are larger than those of the remaining compounds, implying that this compound exhibits stronger deformation resistance and high elastic stiffness in comparison to other studied compounds. This result is expected because the calculated elastic constants of W_5SiB_2 have larger values than their corresponding values for the remaining compounds (see Table II).

Now we investigate the brittle or ductile behavior of the studied superconductors for their possible technological application. Based on the Pugh rule [61], the brittle-or-ductile behavior of a compound can be designated by the ratio of the bulk modulus to the shear modulus (B_H/G_H). If this ratio is greater than its threshold value of 1.75, a compound demonstrates ductility, in contrast if this ratio less than its limit value, a compound shows brittleness. As can be seen from Table III, the calculated B_H/G_H ratios for Mo_5SiB_2, W_5SiB_2, Mo_5GeB_2, and Mo_5PB_2 are 1.898, 2.059, 2.086, and 2.236, respectively, which are above than the limit value. As a consequence, we can state that all the studied compounds are ductile, with Mo_5PB_2 being the most ductile. In addition to two Cauchy pressures and Pugh's ratio, the brittleness and ductility of compounds can be also defined by using Poisson's ratio [62]. If this ratio is smaller (larger) than 0.26, the mechanical property of the material is dominated by brittleness (ductility). Since Poisson's ratio values given in Table III are larger than 0.26, all the studied compounds possess ductile characteristic in agreement with the observations made by the analysis of two Cauchy pressures and Pugh's ratio. Poisson's ratio can also be used to identify the nature of interatomic forces in solids. If the value of this ratio stays between 0.25 and 0.50, compounds can be classified as central force solids; otherwise, they are known as noncentral force solids. Since Poisson's ratio values presented in Table III fall between these boundary values, the central forces of atoms ensure

TABLE IV. Calculated results for the universal anisotropic index (A^u), percent anisotropy (A_B, A_G), transverse (V_T), longitudinal (V_L), average (V_M) elastic wave velocities, and Debye temperature (Θ_D) of all the studied superconductors. Previous experimental and theoretical results are also included for comparison.

Superconductor	A^U	A_B	A_G	V_T (m/s)	V_L (m/s)	V_M (m/s)	Θ_D (K)
Mo_5PB_2	0.2300	0.0025	0.0219	3732.27	7051.02	4160.91	534.21
Experimental [27]							501
GGA [34]	0.1495	0.0026	0.0142	4879.50	9013.06	5398.62	429.09
Mo_5SiB_2	0.1453	0.0014	0.0141	4046.64	7274.77	4046.64	574.08
Experimental [18]							515
GGA [33]				4182.30	7382.90	4650.70	594.0
W_5SiB_2	0.2232	0.0001	0.0218	3062.01	5640.36	3404.73	433.25
Experimental [26]							470
Mo_5GeB_2	0.2979	0.016	0.0286	3656.72	6761.72	4065.39	515.08
Experimental [29]							477

stability in all the studied superconductors which matches with their metallic character. Finally, the ratio of the bulk modulus B_H to the elastic constant C_{44} ($\mu = B_H/C_{44}$) is known as the machinability index of a compound [63]. According to the definition of this index, high overall strength combined with low shear resistance induces good machinability and better dry lubricity. As can be derived from Tables II and III, our calculations produce large values of μ for all four ternary compounds, indicating good machinability for them. This is once again good information for their possible technological applications. Finally, hardness (H) is an important elastic property which is responsible for wear behavior of compounds [64]. The hardness H of all the studied compounds can be estimated by $H = 0.1769G_H - 2.899$ [64]. Table III demonstrates that W_5SiB_2 has the strongest hardness followed by Mo_5SiB_2, Mo_5PB_2 and Mo_5GeB_2. Importantly, the hardness H of all the studied borides is comparable to that of several hard compounds, such as SiC (28 GPa), ZrC (27 GPa), NbC(23 GPa), VN (15 GPa), NbN (14 GPa), and sapphire (Al_2O_3) (22 GPa) [55]. Our theoretical calculations on the elastic and mechanical properties of Mo_5SiB_2, Mo_5GeB_2, Mo_5PB_2, and W_5SiB_2 thus bring to light that they exhibit a matchless combination of high hardness and significant ductility due to their large elastic moduli and considerably positive Cauchy pressures. This observation is very interesting because several conventional superconductors suffer from the problem of low stiffness, which withholds them from a wide range of applications. In view of this, high mechanical stiffness in combination with significant ductility makes all the examined compounds promising candidates for the protection of cutting and forming tools.

Elastic anisotropy affects a variety of physical processes in compounds. Some of these processes comprise the growth of plastic deformation and the creation of microcracks in materials. Several anisotropic indexes are available in the literature but we prefer the universal anisotropic index (A^U) and the percent of anistropy indexes (A_B and A_G), being given via the following equations:

$$A^U = 5\frac{G_V}{G_R} + \frac{B_V}{B_R} - 6 \geqslant 0, \tag{7}$$

$$A_B = \frac{B_V - B_R}{B_V + B_R}, \tag{8}$$

$$A_G = \frac{G_V - G_R}{G_V + G_R}. \tag{9}$$

The calculated values of A^U, A_B, and A_G for all the compounds understudy are listed in Table IV. The anisotropy index factor becomes zero when the compound is completely isotropic while a deviation from zero marks the degree of anisotropy. For all the studied compounds, the value of A_G is significantly larger than that of A_B which is due to a considerable difference in the values of G_V and G_R. This difference influences the value of A^U which is a much better pointer for mechanical anisotropic properties. According to their A^U values given in Table IV, all the examined superconductors are elastically anisotropic.

The Debye temperature (Θ_D), a characteristic temperature, can be utilized to judge many physical properties of compounds, involving thermal expansion, thermal conductivity, lattice vibrations, melting temperature, and specific heat. It is also connected to the superconducting transition temperature and the electron-phonon coupling constant in the case of superconductors [53]. The Debye temperature of a compound linearly depends on the averaged sound velocity (V_M) with the following equation [65]:

$$\Theta_D = \frac{h}{k}\left(\frac{3n}{4\pi}\frac{N_A\rho}{M}\right)^{1/3} V_M, \tag{10}$$

where h, k, n, N_A, M, and ρ represent the Planck's constant, Boltzmann's constant, the number of atoms in the molecule, Avogadro's number, the molecular weight and the mass density of the compound, respectively. The value of V_M can be calculated by the help of transverse and longitudinal acoustic velocities (V_{TA} and V_{LA}) [65]:

$$V_M = \left[\frac{1}{3}\left(\frac{2}{V_T^3} + \frac{1}{V_L^3}\right)\right]^{-1/3}, \tag{11}$$

$$V_L = \left(\frac{3B_H + 4G_H}{3\rho}\right)^{1/2}, \tag{12}$$

$$V_T = \left(\frac{G_H}{\rho}\right)^{1/2}. \tag{13}$$

The calculated values of V_T, V_L, V_M, and Θ_D for all the studied compounds and their comparison with existing

experimental [18,26,27,29] and theoretical [34] results are summarized in Table IV. The Debye temperatures of all compounds examined are consistent with their experimental values [18,26,27,29]. Good agreement with experiment confirms the reliability of this theoretical study. At the same time, there is a physical explanation for this satisfactory harmony because at low temperature the vibrational excitation arises merely from acoustic modes and the long-wave acoustic phonon spectrum is profoundly associated with the elastic constants. In general, a higher Debye temperature signals a higher thermal conductivity [66]. According to Table IV, among all the investigated superconductors, Mo_5SiB_2 has the highest Debye temperature of 574.08 K which indicates relatively high thermal conductivity in Mo_5SiB_2.

C. Phonons and electron-phonon interaction

It is well known that superconductivity in terms of the BCS model relies on the coupling of electrons to lattice vibrations, which makes the knowledge of the lattice dynamics very important for superconductors. Therefore, to identify the underlying pairing mechanism of superconductivity, we have performed phonon and electron-phonon calculations using the density functional perturbation theory.

The calculated phonon dispersion relations for Mo_5SiB_2 are displayed in Fig. 5(a) while associated total and partial phonon density of states (DOS) are plotted in Fig. 5(b). The unit cell of each studied compounds has 16 atoms and thus there are 48 phonon branches. All the phonon branches of this compound have positive frequencies, meaning that it is dynamically stable in its body-centered tetragonal Cr_5B_3-type crystal structure. The phonon dispersion spectrum can be divided into seven regions separated by six gaps of 3.01, 0.71, 0.87, 0.09, 0.87, and 0.94 THz, respectively: part one comprises the lowest thirty Mo-characterized phonon branches ranging from 0 to 7.45 THz, part 2 contains two Si-characterized phonon branches between 10.46 and 10.98 THz, part 3 has four almost flat Si-characterized phonon branches between 11.69 and 12.04 THz, causing a strongest peak at 11.86 THz in the phonon DOS and the remaining parts contain two, two, four and four less dispersive B-characterized phonon branches, respectively, giving rise to significant peaks at 13.43, 14.11, 15.34, 15.71, 16.91, and 17.24 THz in the phonon DOS. Clearly, Mo, Si, and B atoms are vibrationally active in different phonon frequency ranges.

The calculated phonon dispersion relations for Mo_5GeB_2 are shown in Fig. 6(a) while associated total and partial phonon density of states are presented in Fig. 6(b). As can be seen from these figures, the replacement of the Ge atom with the Si atom in Mo_5SiB_2 results in observable modifications in the phonon spectrum and phonon density of states. First, the total width of the phonon spectrum decreases from 17.50 to 17.06 THz due to the heavier mass of the Ge atom compared to Si. Secondly, the vibrations of the second heavy atom (Ge) disappear above the first gap region. Therefore Ge hybridizes with Mo in the first region between 7.18 and 8.54 THz. However, it is worth to mention that this kind of hybridization is not present for Mo_5SiB_2, leaving 30 Mo-based phonon branches totally separated from 6 Si-based phonon branches. Finally, for Mo_5GeB_2, in agreement with Mo_5SiB_2,

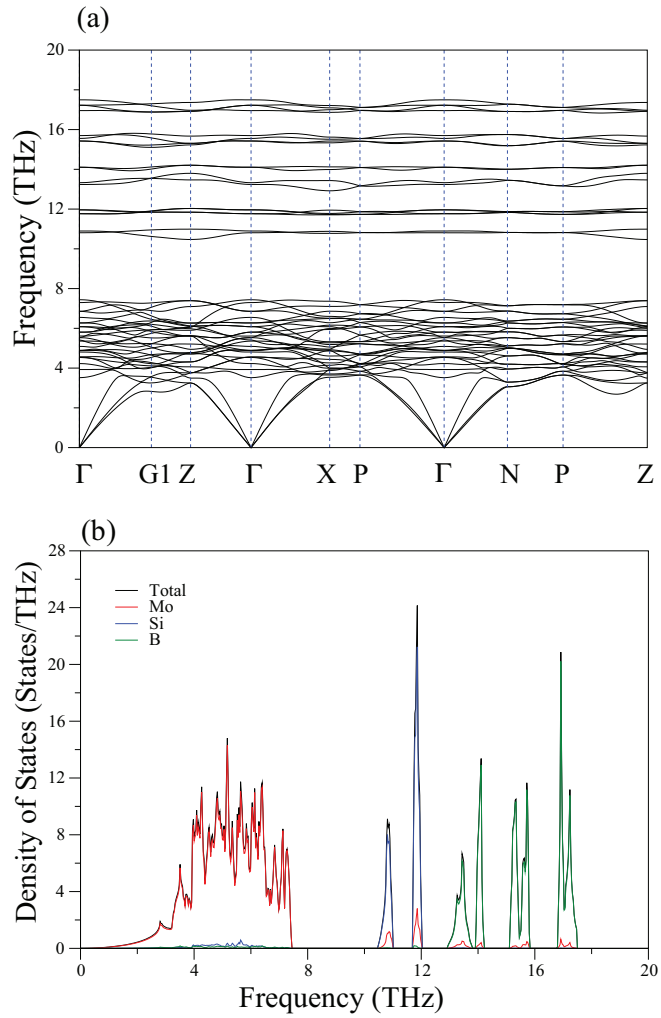

FIG. 5. (a) The calculated phonon spectrum of Mo_5SiB_2 along symmetry lines of the body-centered tetragonal Brillouin zone. (b)The calculated phonon total and partial density of states for Mo_5SiB_2.

12 B-based phonon branches have a remarkably flat dispersion, leading to pronounced peaks in the phonon DOS at higher frequencies 12.87, 14.15, 15.04, 15.61, 16.55, and 16.97 THz, being almost equal to the frequencies of their corresponding counter-patterns in the phonon DOS of Mo_5SiB_2.

The calculated phonon dispersion relations for W_5SiB_2 are shown in Fig. 7(a) while associated total and partial phonon density of states are presented in Fig. 7(b). First, the substitution of Mo atoms with W atoms in Mo_5SiB_2 makes the 30 phonon branches of the low frequency region much softer due to the heavier mass of W compared to that of Mo. Hereat, the width of this frequency region diminishes from 7.45 to 5.80 THz by around 28%. These softer phonon branches may decrease the ω_{ln} value of W_5SiB_2 compared to that of Mo_5SiB_2 but they will definitely make the electron-phonon interaction in W_5SiB_2 stronger than that in Mo_5SiB_2 due to the factor of $1/\omega$ in Eq. (2). Secondly, because of the larger mass difference between W and Si atoms compared to that between Mo and Si atoms, the width of first gap region increases from 3.01 to 4.48 THz. Thirdly, DOS peaks formed by the vibrations of Si and B

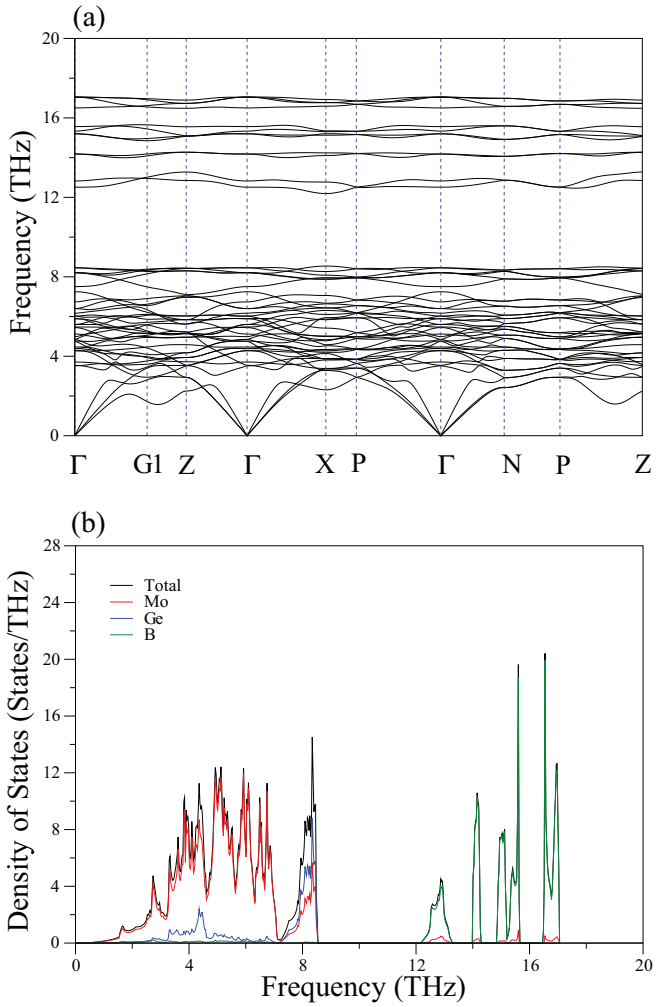

FIG. 6. (a) The calculated phonon spectrum of Mo_5GeB_2 along symmetry lines of the body-centered tetragonal Brillouin zone. (b) The calculated phonon total and partial density of states for Mo_5GeB_2.

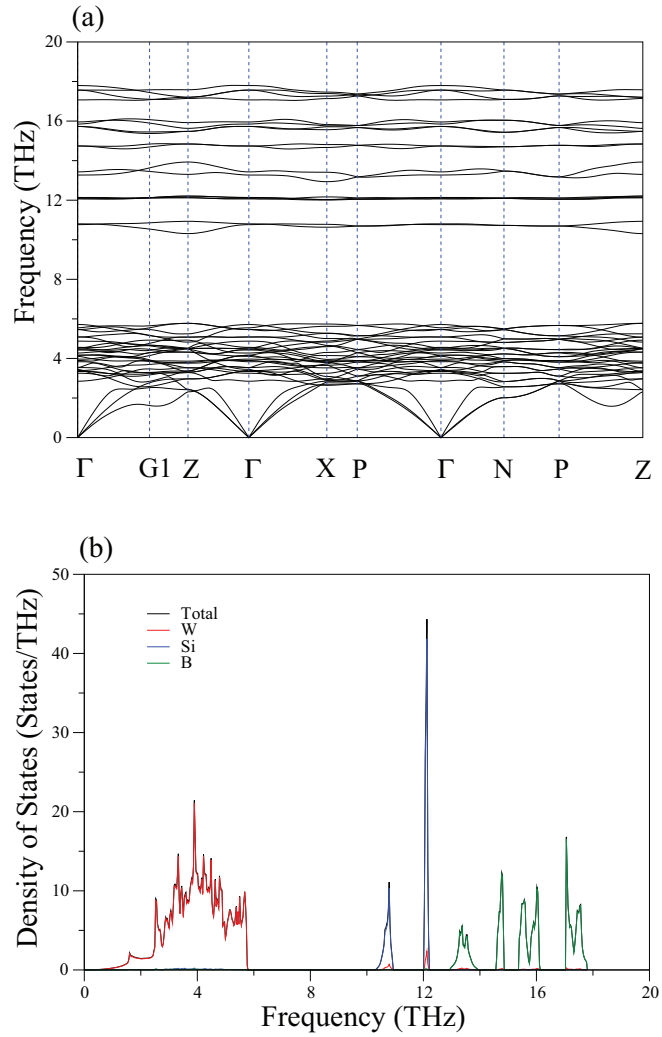

FIG. 7. (a) The calculated phonon spectrum of W_5SiB_2 along symmetry lines of the body-centered tetragonal Brillouin zone. (b) The calculated phonon total and partial density of states for W_5SiB_2.

atom have almost similar frequencies and features with their corresponding counter-patterns in Mo_5SiB_2.

The calculated phonon dispersion relations for Mo_5PB_2 are shown in Fig. 8(a) while associated total and partial phonon density of states are presented in Fig. 8(b). Considering the phonon dispersion in Fig. 8(a), we find that Mo_5PB_2 is also dynamically stable like other borides. The replacement of Si atoms by P atoms almost does not change the width of the first region but this atomic replacement reduces the frequency of the first gap from 3.01 to 1.04 THz, while increasing the frequency of the third gap from 0.87 to 3.20 THz. As a result of these changes, P-related peaks appear at lower frequencies than Si-related peaks. Furthermore, the very low frequency gap of 0.09 THz disappears when the P atoms are placed in the positions of the Si atoms. Once again, the frequencies of B-related peaks for both compounds are close to each other. Different from phonon dispersion curves of above superconductors, the most outstanding feature of phonon dispersion curves for Mo_5PB_2 is the softening of the lowest acoustic branch about halfway along Γ-*G*1-*Z* (at $\boldsymbol{q} \simeq \frac{2\pi}{a}(0.5, 0.0, 0.0)$). Frequently, this kind of phonon softening in the normal state favors superconductivity because the soft phonon mode has the potential to cause an increase in the value of electron-phonon coupling parameter (λ) according to the McMillan-Hopfield expression [50]. The formula of this expression is

$$\lambda = \frac{N(E_F)\langle I^2\rangle}{M\langle\omega^2\rangle}, \tag{14}$$

where $\langle\omega^2\rangle$, $\langle I^2\rangle$, and M refer to the averaged square of the phonon frequency, the averaged square of the electron-phonon matrix element, and the mass involved, respectively. The above expression demonstrates that a sudden decrease in the frequency of the phonon mode can cause an increase in the value of the electron-phonon coupling parameter. In order to bring to light the connection between the phonon softening of the lowest acoustic branch and electron-phonon interaction, the wave-vector dependence of the electron-phonon coupling parameter for this phonon branch is shown in Fig. 8(c). This phonon branch behaves normally showing a positive

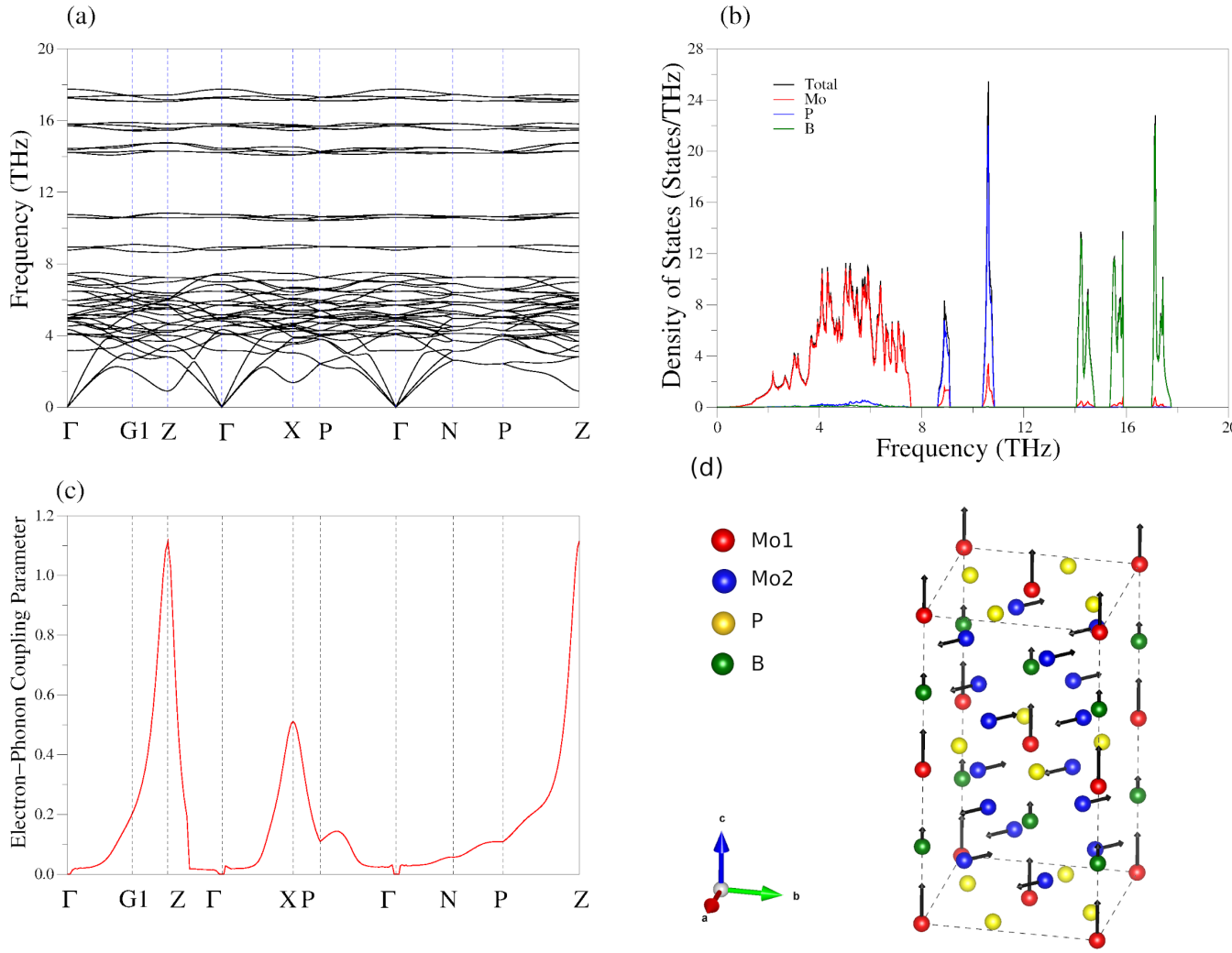

FIG. 8. (a) The calculated phonon spectrum of Mo_5PB_2 along symmetry lines of the body-centered tetragonal Brillouin zone. (b) The calculated phonon total and partial density of states for Mo_5PB_2. (c) The wave-vector dependence of the electron-phonon coupling parameter for the lowest acoustic branch. (d) A schematic illustration of the eigendisplacement pattern of the lowest acoustic phonon mode at the Z point.

dispersion with increasing wave vector along the Γ-$G1$-Z direction close to Γ. However, this phonon mode surprisingly starts to show a negative dispersion (phonon anomaly) beyond $\boldsymbol{q} \simeq \frac{2\pi}{a}$ (0.5, 0.0, 0.00) along the Γ-G1-Z direction. Therefore this phonon branch has a clear minimum at the zone boundary of Z with a frequency of 2.25 THz. However, the electron-phonon interaction parameter of this phonon branch still continues to increase rapidly and reaches its maximum value of 1.12 at the Z point. As a consequence, this observation reveals a positive relationship between phonon anomaly and electron-phonon coupling parameter. Figure 8(d) depicts a schematic illustration of the eigendisplacement pattern of lowest acoustic phonon mode at the Z point. This phonon mode is mainly dominated by the vibrations of Nb atoms, and the states near the Fermi level are almost totally dominated by their d states. Thus the displacement pattern of this phonon mode gives rise to significant changes in the overlap of electronic orbitals, leading a large electron-phonon coupling parameter. It is worth to mention that similar observation is made for this phonon mode at the X point. On the other hand, this type of phonon anomaly has not been observed in the lowest acoustic modes of other borides. As a consequence, we believe that this phonon anomaly makes the electron-phonon interaction stronger in Mo_5PB_2 than that in other borides, resulting in its T_c value being higher than the T_c values of other borides.

A major aim of our *ab initio* calculations is to analyze the strength of the electron-phonon coupling in all four borides, which is calculated from an integral of Eliashberg function $\alpha^2F(\omega)$ times $1/\omega$ over phonon frequency [see Eq. (2)]. Figure 9 depicts the calculated Eliashberg functions $\alpha^2F(\omega)$ of all four borides along with their frequency accumulative electron-phonon coupling parameter $\lambda_{\rm acc}(\omega)$. As expected, each $\alpha^2F(\omega)$ function pursues its corresponding phonon density of states because this function consists of two parts $F(\omega)$ and α^2; $F(\omega)$ is similar to the phonon density of states and α^2 contains an average square electron-phonon matrix element. As expected from the dominance of transition metal d electrons at the Fermi level, the combination of phonon density of states and Eliashberg spectral functions shows that vibrations with a strong electron-phonon coupling are dominated by transition metal atoms in the low-frequency

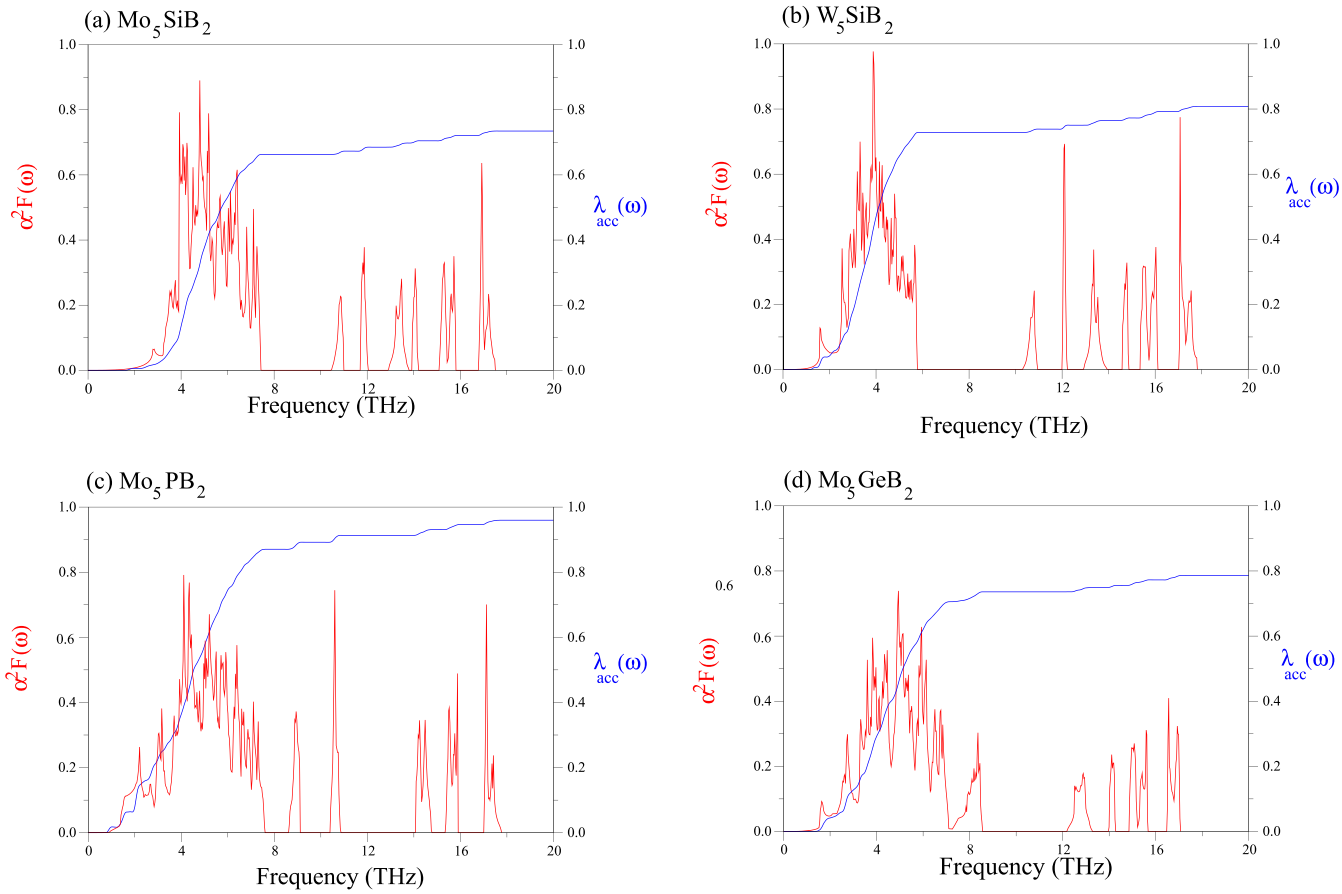

FIG. 9. The Eliashberg spectral function $\alpha^2F(\omega)$ and the frequency accumulative electron-phonon coupling parameter $\lambda_{acc}(\omega)$ for (a) Mo_5SiB_2, (b) W_5SiB_2, (c) Mo_5PB_2, and (d) Mo_5GeB_2.

region, leading to several peaks in the low-frequency region of $\alpha^2F(\omega)$, causing a much faster increase in $\lambda_{acc}(\omega)$ in the first frequency region compared to other frequency regions. In particular, combining the phonon density of states and the frequency accumulative electron-phonon coupling parameter $\lambda_{acc}(\omega)$ (see Fig. 9) for Mo_5SiB_2, W_5SiB_2 and Mo_5PB_2, we are able to reach the conclusion that low-frequency phonons almost totally contributed by transition metal atoms, play a dominant role in the transition from the normal state to the superconducting state arising from their large contribution to λ (90% for the first two compounds and 91% for the third compound), and the remaining is contributed by intermediate frequency Si (P) phonon modes (3% for the first two compounds and 4% for the third compound) and high-frequency B phonon mode (7% for the first two compounds and 5% for the third compound). As we mentioned before, the second element hybridizes with the transition metal atom in Mo_5GeB_2 with almost equal weights, whereas in the above compounds there is no hybridization, leaving all atomic vibrations entirely separated. Therefore low-frequency optical phonons between 7.18 and 8.54 THz, jointly contributed by Mo and Ge atoms, form 4% of total λ, while Mo-related vibrations below 7.18 THz offer almost 90% to total λ, and the remaining is contributed by high-frequency phonons associated with B vibrations. These contributions emphasize that transition metal-induced vibrations strongly mediate the formation of Cooper pairs while other vibrations are negligibly involved in the process of scattering of electrons. This picture is expected because for all the studied borides, almost 90% of total λ is formed by the vibrations of transition metal atoms, being in full agreement with our electronic results indicating that almost the same percentage of $N(E_F)$ originates from their d states.

By using McMillan-Allen-Dynes formula [see Eq. (4)], the calculated λ and the calculated ω_{ln}, we are able to estimate the T_c values for all the studied borides, as listed in Table V together with their $N(E_F)$, λ, and ω_{ln} values. First of all, one can see that the calculated T_c values for Mo_5SiB_2 (5.845 K), W_5SiB_2 (5.931 K), Mo_5GeB_2 (6.193 K), and Mo_5PB_2 (9.527 K) harmonize with their corresponding experimental values (see Table V), supporting the validity of our theoretical approach. As we mentioned before, the change of the transition metal from Mo to W affects the results of phonon and electron-phonon interaction. Thus first the results obtained for compounds containing Mo will be compared and discussed. Both $N(E_F)$ and λ values calculated for Mo_5PB_2 are higher than those of other Mo-containing compounds. It is well known that both physical quantities make positive contribution to the value of T_c and thus the T_c value of Mo_5PB_2 becomes highest among all studied compounds due to its highest $N(E_F)$ and λ values. Similarly, the calculated T_c value of Mo_5GeB_2 is higher than that of Mo_5SiB_2 because both its $N(E_F)$ and λ value are higher than those of Mo_5SiB_2. As a result, differences in T_c values of Mo-containing

TABLE V. The calculated values of density of states at the Fermi level [$N(E_F)$], average electron-phonon coupling constant (λ), logarithmically averaged phonon frequency ($\omega_{\ln}$), and superconducting critical temperature (T_c).

Superconductor	N(E_F) (states/eV)	λ	ω_{ln} (K)	T_c (K)
Mo_5PB_2	10.317	0.959	206.314	9.527
Experimental [27]		1.01		9.2
GGA [27]	10.70			
Mo_5SiB_2	10.022	0.735	255.351	5.845
Experimental [18,27]		0.73		5.8
W_5SiB_2	8.512	0.808	194.590	5.931
Experimental [26]				5.8
Mo_5GeB_2	10.143	0.786	220.243	6.193
Experimental [29]		0.57		5.4
Experimental [30]		0.65		5.8

compounds can be explained by differences in their N(E_F) and λ values. However, although the N(E_F) and ω_{ln} values of W_5SiB_2 (8.512 states/eV and 194.590 K) are lower than those of Mo_5SiB_2 (10.022 states/eV and 255.351 K), and Mo_5GeB_2 (10.143 states/eV and 220.243 K), its calculated T_c value of 5.931 K is slightly higher and lower than that of Mo_5SiB_2 ($T_c = 5.845$ K) and Mo_5GeB_2 ($T_c = 6.193$ K), respectively. We are able to explain this situation in that the heavier mass of the W atoms shifts the Eliashberg function to a lower phonon frequency range, where it contributes more effectively to the electron-phonon coupling constant (λ). As a consequence, the electron-phonon interaction in W_5SiB_2 becomes slightly stronger than that in Mo_5SiB_2 and Mo_5GeB_2 but the higher ω_{ln} values of Mo_5SiB_2 and Mo_5GeB_2 mitigate this discrepancy, making their T_c values almost equal. As a result, in this work, using first-principles calculations of electronic structure, phonons, and their interaction, we have demonstrated that superconductivity in all the studied borides is conventional phonon-mediated in nature.

IV. SUMMARY

In this paper, we have presented a comprehensive first-principles study on the structural, electronic, elastic, mechanical, phonon and electron-phonon interaction properties of Mo_5SiB_2, Mo_5GeB_2, Mo_5PB_2, and W_5SiB_2 compounds, in the hope of uncovering the origin of superconductivity for them by using the density functional theory within a generalized gradient approximation.

The calculated lattice parameters and internal coordinates compare very well with their corresponding experimental values. The calculated electronic band structures reveal that all the considered borides are metals in their normal state. A common feature of the investigated compounds is a principal role of the transition metal atoms in the formation of superconducting state. With the Fermi level mainly composed of their d states, Cooper pairs in the BCS theory can be formed by electrons having energies close to the Fermi energy. All the calculated elastic constants are found to be positive and follow the Born's mechanical stability criteria of a body-centered tetragonal structure. Our study suggests that they exhibit a matchless combination of high hardness and significant ductility due to their large elastic moduli and considerably positive Cauchy pressures which makes them promising candidates for the protection of cutting and forming tools.

The phonon band structure analysis shows that all the studied compounds are dynamically stable in their body-centered tetragonal Cr_5B_3-type crystal structure. Atomic vibrations are almost completely separated from each other in all except Mo_5GeP_2, which contains almost equal amount of hybridization of Ge and Mo vibrations in the upper part of low-frequency region due the heavier mass of Ge atom compared to that of Si and P atoms. The lowest-frequency branch in Mo_5PB_2 has a particularly strong tendency for softening, probably making the electron-phonon interaction in this compound stronger than that in the compounds studied here.

Mo_5PB_2 has the highest T_c value among all the considered compounds, which is related to its largest λ value arising from the existence of phonon anomaly in its lowest-acoustic phonon branch. Substitution of W by Mo affects the the Eliashberg spectral function by shifting the peaks to lower frequencies due to the heavier mass of W, resulting in increase of λ_{acc} (ω) for W_5SiB_2. The electron-phonon interaction in W_5SiB_2 is stronger than that in Mo_5SiB_2 and Mo_5GeB_2 but the higher ω_{ln} values for Mo_5SiB_2 and Mo_5GeB_2 mitigates this discrepancy, making their T_c values closer to each other. Combining the phonon density of states and the frequency accumulative electron-phonon coupling parameters, we have observed that low-frequency phonons, mainly contributed by transition metal atoms, play a dominant role in the transition from the normal state to the superconducting state for all the studied borides due to their large contribution to λ (around 90%). This large contribution is in full accordance with our electronic results indicating that almost the same percentage of N(E_F) originates from transition metal d states.

Finally, all above interesting results indicate that Mo_5SiB_2, Mo_5GeB_2, Mo_5PB_2, and W_5SiB_2 are hard superconductors with ductile character, and are interesting compounds for studying phenomena originating from the interplay of ductility, hardness and superconductivity.

[1] G. Akopov, M. T. Yeung, and R. B. Kaner, Rediscovering the crystal chemistry of borides, Adv. Mater. **29**, 1604506 (2017).

[2] H. Stadelmaier, N. Elmasry, N. Liu, and S. Cheng, The metallurgy of the iron-neodymium- boron permanent magnet system, Mater. Lett. **2**, 411 (1984).

[3] M. Jones, A. J. Horlock, P. H. Shipway, D. G. McCartney, and J. V. Wood, A comparison of the abrasive wear behaviour of HVOF sprayed titanium carbide-and titanium boride-based cermet coatings, Wear **251**, 1009 (2001).

[4] W. Tang, Q. Wang, S. Wang, and F. Lu, A comparison in performance of diamond coated cemented carbide cutting tools with and without a boride interlayer, Surf. Coat. Technol. **153**, 298 (2002).

[5] C. Martini, G. Palombarini, G. Poli, and D. Prandstraller, Sliding and abrasive wear behaviour of boride coatings, Wear **256**, 608 (2004).

[6] P. A. Dearnley, M. Schellewald, and K. L. Dahm, Characterisation and wear response of metal-boride coated WC-Co, Wear **259**, 861 (2005).

[7] D. M. de Almeida, C. Bormio-Nunes, C. A. Nunes, A. A. Coelho, and G. C. Coelho, Magnetic characterization of Mn_5SiB_2 and Mn_5Si_3 phases, J. Magn. Magn. Mater. **321**, 2578 (2009).

[8] Z. G. Xie, D. Y. Geng, and Z. D. Zhang, Reversible room-temperature magnetocaloric effect in Mn_5PB_2, Appl. Phys. Lett. **97**, 202504 (2010).

[9] E. Sani, L. Mercatelli, D. Jafrancesco, J. Sans, and D. Sciti, Ultra-high temperature ceramics for solar receivers: Spectral and high-temperature emittance characterization, J. Eur. Opt. Soc.: Rap. Public. **7**, 12052 (2012).

[10] J. A. Lemberg and R. O. Ritchie, Mo-Si-B alloys for ultrahigh-temperature structural applications, Adv. Mater. **24**, 3445 (2012).

[11] H. Vrubel and X. Hu, Molybdenum boride and carbide catalyze hydrogen evolution in both acidic and basic solutions, Angew. Chem. Int. Ed. **51**, 12703 (2012).

[12] D. Sciti, L. Silvestroni, L. Mercatelli, J.-L. Sans, and E. Sani, Suitability of ultra-refractory diboride ceramics as absorbers for solar energy applications, Sol. Energy Mater. Sol. Cells **109**, 8 (2013).

[13] M. A. McGuire and D. S. Parker, Magnetic and structural properties of ferromagnetic Fe_5PB_2 and Fe_5SiB_2 and effects of Co and Mn substitutions, J. Appl. Phys. **118**, 163903 (2015).

[14] T. N. Lamichhane, V. Taufour, S. Thimmaiahb, D. S. Parker, S. L. Budko, and P. C. Canfield, A study of the physical properties of single crystalline Fe_5B_2P, J. Magn. Magn. Mater. **401**, 525 (2016).

[15] S. Kota, S. E. Zapata-Solvas, A. Ly, J. Lu, O. Elkassabany, A. Huon, W. E. Lee, L. Hultma, S. J. May, and M. W. Barsoum, Synthesis and characterization of an alumina forming nanolaminated boride: MoAlB, Sci. Rep. **6**, 26475 (2016).

[16] H. Hu, Y. Guo, J. Yan, J. Qiu, and Y. Wang, Dry sliding wear behavior of $MoSi_2$-Mo_5Si_3-Mo_5SiB_2 composite at different temperatures and loads, Wear **428–429**, 237 (2019).

[17] J. Nagamatsu, N. Nakagawa, T. Muranaka, Y. Zenitani, and J. Akimitsu, Superconductivity at 39 K in magnesium diboride, Nature (London) **410**, 63 (2001).

[18] A. J. d. S. Machado, A. Costa, C. Nunes, C. Dos Santos, T. Grant, and Z. Fisk, Superconductivity in Mo_5SiB_2, Solid State Commun. **151**, 1455 (2011).

[19] R. D. Field, D. J. Thoma, J. C. Cooley, F. Chu, C. L. Fu, M. H. Yoo, W. L. Hults, and C. M. Cady, Dislocations in Mo_5SiB_2 T2 phase, Intermetallics **9**, 863 (2001).

[20] K. Ihara, K. Ito, K. Tanaka, and M. Yamaguchi, Mechanical properties of Mo_5SiB_2 single crystals, Mater. Sci. Eng. A **329–331**, 222 (2002).

[21] B. Aronsson, The crystal structure of Mo_5SiB_2, Acta Chem. Scand. **12**, 31 (1958).

[22] C. J. Rawn, J. H. Schneibel, C. M. Hoffmann, and C. R. Hubbard, The crystal structure and thermal expansion of Mo_5SiB_2, Intermetallics **9**, 209 (2001).

[23] M.-K. Wu, J. R. Ashburn, C. Torng, P. H. Hor, R. L. Meng, L. Gao, Z. J. Huang, Y. Wang, and A. Chu, Superconductivity at 93 K in a new mixed-phase Y-Ba-Cu-O compound system at ambient pressure, Phys. Rev. Lett. **58**, 908 (1987).

[24] A. Drozdov, M. Eremets, I. Troyan, V. Ksenofontov, and S. I. Shylin, Conventional superconductivity at 203 kelvin at high pressures in the sulfur hydride system, Nature (London) **525**, 73 (2015).

[25] Y. Wang, M. Li, H. Wang, G. Shao, J. Zhu, W. Liu, H. Wang, B. Fan, H. Xu, and H. Lu, The fabrication and mechanical properties of laminated ZrB_2-Mo_5SiB_2 ceramics with an Mo-Mo_5SiB_2 interlayer, Metals **11**, 2018 (2021).

[26] M. Fukuwa, K. K. Awashima, M. M. Aruyama, and J. A. Kimitsu, Superconductivity in W_5SiB_2 with the T_2 phase structure, J. Phys. Soc. Jpn. **80**, 024702 (2011).

[27] M. A. McGuire and D. S. Parker, Superconductivity at 9 K in Mo_5PB_2 with evidence for multiple gaps, Phys. Rev. B **93**, 064507 (2016).

[28] T. Shang, W. Xie, D. J. Gawryluk, R. Khasanov, J. Zhao, M. Medarde, M. Shi, H. Yuan, E. Pomjakushina, and T. Shiroka, Multigap superconductivity in the Mo_5PB_2 boron-phosphorus compound, New J. Phys. **22**, 093016 (2020).

[29] B. Xu, Z. Lou, H. Chen, Y. Zhou, Q. Chen, S. Chen, C. Wu, H. Wang, J. Yang, J. Du, and M. Fang, Superconductivity in Mo_5GeB_2 with a tetragonal structure, Supercond. Sci. Technol. **34**, 035030 (2021).

[30] B.-B. Ruan, Q.-S. Yang, M.-H. Zhou, G.-F. Chen, and Z.-A. Ren, Superconductivity in a new T2-phase Mo_5GeB_2, J. Alloys Compd. **868**, 159230 (2021).

[31] S. Kim and J. Park, *Ab initio* calculated thermodynamic properties of Mo_5SiB_2 phase and Nb_5SiB_2 phase, JOM **65**, 1482 (2013).

[32] S. Aryal, M. Gao, L. Ouyang, P. Rulis, and W. Ching, *Ab initio* studies of Mo-based alloys: Mechanical, elastic, and vibrational properties, Intermetallics **38**, 116 (2013).

[33] Y. Pan and D. Pu., Influence of vacancy on the mechanical, electronic and thermodynamic properties of Mo_5SiB_2 from first-principles calculations, J. Electron. Mater. **49**, 1282 (2020).

[34] M. I. Naher, M. A. Afzal, and S. H. Naqib, A comprehensive DFT based insights into the physical properties of tetragonal superconducting Mo_5PB_2, Results Phys. **28**, 104612 (2021).

[35] D. Pu and Y. Pan, New insight into the structural stability, ductility and melting point of Mo_5SiB_2 under high-pressure environment, Vacuum **196**, 110727 (2022).

[36] P. Giannozzi, S. Baroni, N. Bonini, M. Calandra, R. Car, C. Cavazzoni, D. Ceresoli, G. L. Chiarotti, M. Cococcioni, I. Dabo, A. Dal Corso, S. de Gironcoli, S. Fabris, G. Fratesi, R. Gebauer, U. Gerstmann, C. Gougoussis, A. Kokalj, M. Lazzeri, L. Martin-Samos, N. Marzari *et al.*, QUANTUM ESPRESSO: A modular and open-source software project for quantum simulations of materials, J. Phys.: Condens. Matter **21**, 395502 (2009).

[37] P. Giannozzi, O. Andreussi, T. Brumme, O. Bunau, M. Buongiorno Nardelli, M. Calandra, R. Car, C. Cavazzoni, D. Ceresoli, M. Cococcioni, N. Colonna, I. Carnimeo, A. Dal Corso, S. de Gironcoli, P. Delugas, R. A. DiStasio Jr., A. Ferretti, A. Floris, G. Fratesi, G. Fugallo, R. Gebauer, U. Gerstmann, F. Giustino, S. Poncé *et al.*, Advanced capabilities for materials modelling with Quantum ESPRESSO, J. Phys.: Condens. Matter **29**, 465901 (2017).

[38] A. Dal Corso, Elastic constants of beryllium: A first-principles investigation, J. Phys.: Condens. Matter **28**, 075401 (2016).
[39] W. Voigt, Lehrbuch der Kristallphysik, Leipzig, Taubner, Adv. Earth Sci. (1928).
[40] A. Reuss, Berechnung der fließgrenze von mischkristallen auf grund der plastizitätsbedingung für einkristalle, Z. Angew. Math. Mech. **9**, 49 (1929).
[41] R. Hill, The elastic behaviour of a crystalline aggregate, Proc. Phys. Soc. Sect. A **65**, 349 (1952).
[42] Z.-J. Wu, E.-J. Zhao, H.-P. Xiang, X.-F. Hao, X.-J. Liu, and J. Meng, Crystal structures and elastic properties of superhard IrN_2 and IrN_3 from first principles, Phys. Rev. B **76**, 054115 (2007).
[43] A. B. Migdal, Interaction between electrons and lattice vibrations in a normal metal, Sov. Phys. JETP **7**, 996 (1958).
[44] G. M. Eliashberg, Interaction between electrons and lattice vibrations in a superconductor, Sov. Phys. JETP **11**, 696 (1960).
[45] P. Hohenberg and W. Kohn, Inhomogeneous electron gas, Phys. Rev. **136**, B864 (1964).
[46] W. Kohn and L. J. Sham, Self-consistent equations including exchange and correlation effects, Phys. Rev. **140**, A1133 (1965).
[47] J. P. Perdew, K. Burke, and M. Ernzerhof, Generalized gradient approximation made simple, Phys. Rev. Lett. **77**, 3865 (1996).
[48] D. Vanderbilt, Soft self-consistent pseudopotentials in a generalized eigenvalue formalism, Phys. Rev. B **41**, 7892 (1990).
[49] H. J. Monkhorst and J. D. Pack, Special points for Brillouin-zone integrations, Phys. Rev. B **13**, 5188 (1976).
[50] W. L. McMillan, Transition temperature of strong-coupled superconductors, Phys. Rev. **167**, 331 (1968).
[51] P. B. Allen and R. C. Dynes, Transition temperature of strong-coupled superconductors reanalyzed, Phys. Rev. B **12**, 905 (1975).
[52] P. B. Allen and R. C. Dynes, Superconductivity at very strong coupling, J. Phys. C: Solid State Phys. **8**, L158 (1975).
[53] J. P. Carbotte, Properties of boson-exchange superconductors, Rev. Mod. Phys. **62**, 1027 (1990).
[54] F. D. Murnaghan, The compressibility of media under extreme pressures, Proc. Natl. Acad. Sci. USA **30**, 244 (1944).
[55] D. M. Teter, Computational alchemy: The search for new superhard materials, MRS Bull. **23**, 22 (1998).
[56] E. Knittle, R. M. Wentzcovitch, R. Jeanloz, and M. L. Cohen, Experimental and theoretical equation state of cubic boron nitride, Nature (London) **337**, 349 (1989).
[57] S. Y. Savrasov, D. Y. Savrasov, and O. K. Andersen, Linear-response calculations of electron-phonon interactions, Phys. Rev. Lett. **72**, 372 (1994).
[58] S. Y. Savrasov and D. Y. Savrasov, Electron-phonon interactions and related physical properties of metals from linear-response theory, Phys. Rev. B **54**, 16487 (1996).
[59] A. Kokalj, XCRYSDEN-a new program for displaying crystalline structures and electron densities, J. Mol. Graphics Modell. **17**, 176 (1999).
[60] D. G. Pettifor, Theoretical predictions of structure and related properties of intermetallics, Mater. Sci. Technol. **8**, 345 (1992).
[61] S. Pugh, XCII. Relations between the elastic moduli and the plastic properties of polycrystalline pure metals, Philos. Mag. **45**, 823 (1954).
[62] J. Haines, J. Leger, and G. Bocquillon, Synthesis and design of superhard materials, Annu. Rev. Mater. Res. **31**, 1 (2001).
[63] Z. Sun, D. Music, R. Ahuja, and J. M. Schneider, Theoretical investigation of the bonding and elastic properties of nanolayered ternary nitrides, Phys. Rev. B **71**, 193402 (2005).
[64] A. Bouhemadou, D. Allali, S. Bin-Omran, E. M. A. Al Safi, R. Khenata, and Y. Al-Douri, Elastic and thermodynamic properties of the SiB_2O_4 (B = Mg, Zn and Cd) cubic spinels: An *ab initio* FP-LAPW study, Mater. Sci. Semicond. Process. **38**, 192 (2015).
[65] O. L. Anderson, A simplified method for calculating the Debye temperature from elastic constants, J. Phys. Chem. Solids **24**, 909 (1963).
[66] G. P. Srivastava, *The Physics of Phonons*, 2nd ed. (CRC Press, Boca Raton, 2022).